

Effect of short-term plasticity on working memory

Fan Yang(杨帆) and Feng Liu(刘锋)
Citation: Chin. Phys. B, 2023, 32 (**11**): 118706. DOI: 10.1088/1674-1056/acf03a
Journal homepage: http://cpb.iphy.ac.cn; http://iopscience.iop.org/cpb

What follows is a list of articles you may be interested in

Fitness of others' evaluation effect promotes cooperation in spatial public goods game

Jian-Wei Wang(王建伟), Rong Wang(王蓉), and Feng-Yuan Yu(于逢源)
Chin. Phys. B, 2021, 30 (**12**): 128701. DOI: 10.1088/1674-1056/ac05ae

Magnetic-resonance image segmentation based on improved variable weight multi-resolution Markov random field in undecimated complex wavelet domain

Hong Fan(范虹), Yiman Sun(孙一曼), Xiaojuan Zhang(张效娟), Chengcheng Zhang(张程程), Xiangjun Li(李向军), and Yi Wang(王乙)
Chin. Phys. B, 2021, 30 (**7**): 078703. DOI: 10.1088/1674-1056/abe1a2

Benefit community promotes evolution of cooperation in prisoners' dilemma game

Jianwei Wang(王建伟), Jialu He(何佳陆), Fengyuan Yu(于逢源), Wei Chen(陈伟), Rong Wang(王蓉), Ke Yu(于可)
Chin. Phys. B, 2019, 28 (**10**): 108703. DOI: 10.1088/1674-1056/ab3f1e

Individual identification using multi-metric of DTI in Alzheimer's disease and mild cognitive impairment

Ying-Teng Zhang(张应腾), Shen-Quan Liu(刘深泉)
Chin. Phys. B, 2018, 27 (**8**): 088702. DOI: 10.1088/1674-1056/27/8/088702

Self-sustained firing activities of the cortical network with plastic rules in weak AC electrical fields

Qin Ying-Mei(秦迎梅), Wang Jiang(王江), Men Cong(门聪), Zhao Jia(赵佳), Wei Xi-Le(魏熙乐), and Deng Bin(邓斌)
Chin. Phys. B, 2012, 21 (**7**): 078702. DOI: 10.1088/1674-1056/21/7/078702

Effect of short-term plasticity on working memory

Fan Yang(杨帆) and Feng Liu(刘锋)[†]

Department of Physics and Institute for Brain Sciences, Nanjing University, Nanjing 210093, *China*

(Received 20 April 2023; revised manuscript received 30 June 2023; accepted manuscript online 15 August 2023)

The way in which persistent firing activity and synaptic plasticity are orchestrated to underlie working memory in recurrent neural networks is not fully understood. Here, we build a continuous attractor network of pyramidal cells and interneurons to simulate an oculomotor delayed response task. Both short-term facilitation (STF) and short-term depression (STD) manifest at synapses between pyramidal cells. The efficacy of individual synapses depends on the time constants of STF and STD as well as the presynaptic firing rate. Self-sustained firing activity (i.e., a bump attractor) during the delay period encodes the cue position. The bump attractor becomes more robust against random drifts and distractions with enhancing STF or reducing STD. Keeping STF and STD at appropriate levels is crucial for optimizing network performance. Our results suggest that, besides slow recurrent excitation and strong global inhibition, short-term plasticity plays a prominent role in facilitating mnemonic behavior.

Keywords: bump attractor, synaptic plasticity, robustness, sensitivity

PACS: 87.19.lj, 87.19.lw, 87.18.Sn **DOI:** 10.1088/1674-1056/acf03a

1. Introduction

Working memory (WM) refers to the brain function of holding and manipulating information over short time periods and is involved in diverse cognitive behaviors such as reasoning, decision making and learning.[1–4] Oculomotor delayed response (ODR) task is a classical experimental paradigm for working memory, where an animal is trained to saccade in the direction indicated by a cue presented seconds earlier.[5,6] During the interval between cue removal and action initiation, i.e. the delay period, selective neurons in the dorsolateral prefrontal cortex (PFC) exhibit elevated spiking activity. It has been proposed that this persistent firing underlies spatial working memory.[5,7]

The self-sustained activity in a recurrent neural network is often manifested as a bump attractor, arising from the interplay between local excitation and global inhibition.[7] Typically, the interaction between activated pyramidal cells, mediated by NMDA receptors, forms a self-reinforcing mechanism characterized by slow dynamics, enabling the sustained firing of these cells. Simultaneously, the inhibition exerted by interneurons through GABA receptors ensures global control and facilitates a winner-takes-all mechanism within the network.

Notably, synaptic plasticity, particularly short-term plasticity (STP), is also recognized as playing a role in the maintenance of WM. For example, short-term facilitation (STF) enhances the ability of a neural circuit to sustain persistent activity following a transient stimulus.[8] The slow dynamics of STP allow tuning the tradeoff between accuracy and flexibility in a WM circuit.[9] Interestingly, STP has been implicated in memory biases resulting from the previous experiment[10,11] and supports an activity-silent mechanism of WM.[12] Thus, although persistent firing is widely accepted as the substrate of WM, the influence of STP on WM cannot be overlooked.

It was reported that STF has a stabilizing effect on WM, in contrast to short-term depression (STD) in a firing rate based model.[13] However, the impact of STP on cue detection sensitivity and memory storage against distraction remains unclear. To this end, we built a spiking neural network to examine the mechanisms underlying WM in the ODR task. Our analysis dissects the contributions of STF and STD to the stability of memory storage and the network's sensitivity to cue presentation. This study indicates that appropriate levels of STP are required to ensure robust memory maintenance.

2. Methods

2.1. Network model

To recapitulate the mnemonic behavior on the ODR task, we constructed a recurrent network model in a manner similar to that in Ref. [7]. The network consists of 2048 pyramidal cells (E) and 512 interneurons (I) [Fig. 1]. All neurons are labeled by their preferred directions, which are uniformly distributed between 0° and 360°. Neurons are recurrently connected; the connections between pyramidal cells are structured, while the others are uniform.

Both pyramidal cells and interneurons are described by the leaky integrate-and-fire (LIF) model. The membrane potential $V_{\rm m}(t)$ of each neuron obeys

$$C_{\rm m}\frac{{\rm d}V_{\rm m}(t)}{{\rm d}t} = -g_{\rm L}\left(V_{\rm m}(t)-V_{\rm L}\right) - I_{\rm rec}(t) - I_{\rm bg}(t) + I_{\rm stim}(t), \quad (1)$$

where $C_{\rm m}$, $g_{\rm L}$ and $V_{\rm L}$ denote the membrane capacitance, leaky

[†]Corresponding author. E-mail: fliu@nju.edu.cn

© 2023 Chinese Physical Society and IOP Publishing Ltd

conductance and resting potential, respectively. $I_{\rm rec}$ is the total amount of recurrent currents in the network, and $I_{\rm bg}$ denotes the random background inputs from neurons outside the network. During a specific time period, only a subset of pyramidal cells receives a stimulus $I_{\rm stim}$, representing a cue- or distractor-related input. The neuron generates a spike whenever its membrane potential reaches a threshold $V_{\rm th}$, followed by a reset to $V_{\rm res}$ during a refractory period ($\tau_{\rm ref}$). For pyramidal cells, $C_{\rm m} = 0.5$ nF, $g_{\rm L} = 25$ nS, $V_{\rm L} = -70$ mV, $V_{\rm th} = -50$ mV, $V_{\rm res} = -60$ mV and $\tau_{\rm ref} = 2$ ms; for interneurons, $C_{\rm m} = 0.2$ nF, $g_{\rm L} = 20$ nS, $V_{\rm L} = -70$ mV, $V_{\rm th} = -50$ mV, $V_{\rm res} = -60$ mV and $\tau_{\rm ref} = 1$ ms. The ordinary differential equations were integrated using a second-order Runge–Kutta algorithm, with a time step of 0.1 ms.

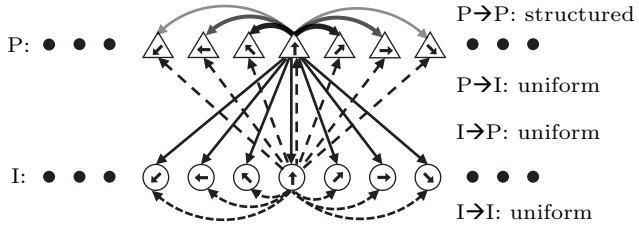


Fig. 1. Schematic of the ring attractor network model. Pyramidal cells and interneurons are uniformly distributed on a separate ring, with their preferred directions indicated by labeled short arrows. Pyramidal cells with more similar preferred directions have stronger connectivity strength, as reflected by the depth of the arrows.

The input $I_{\rm stim}$ is modeled as an injected current to pyramidal cells: $I_{\rm stim}(\theta) = I_0 \exp[-(\theta-\theta_{\rm s})^2/2\sigma_{\rm s}^2]$, where $\theta_{\rm s}$ labels the direction of a cue or distractor, and $\sigma_{\rm s}$ represents its width and is always set to 18°. $\theta_{\rm s}$ varies in different situations, and $I_0 = 500$ pA unless otherwise specified. In simulation, the cue always appears at 75 ms and lasts 250 ms; on some trials, the distractor appears at 375 ms, with the same strength, width and duration as the cue but at a distinct position.

Different from the stimulus input, both recurrent currents and background inputs are transmitted by synapses. Excitatory postsynaptic currents (EPSCs) are mediated by NMDA receptors (NMDARs) and AMPA ones (AMPARs), while inhibitory currents are mediated by $\rm GABA_A$ receptors (GABARs). Considering that NMDAR-mediated recurrent currents have proved indispensable for sustained activity in working memory,[14,15] here recurrent excitatory currents are purely NMDAR-driven for simplicity, and background synaptic currents are solely AMPAR-controlled, as in Ref. [7].

For neuron i, $I_{\rm rec} = I_{i,\rm NMDA} + I_{i,\rm GABA}$ and $I_{\rm bg} = I_{i,\rm AMPA}$, with

$$I_{i,\rm NMDA} = (V_i - V_{\rm E}) \frac{\sum_j p_{j,\rm NMDA} g_{ji,\rm NMDA} s_{j,\rm NMDA}}{1 + \left[{\rm Mg}^{2+}\right] \exp\left(-0.062 V_i\right)/3.57}, \quad (2)$$

$$I_{i,\rm AMPA} = (V_i - V_{\rm E})\, G_{\rm ext} \sum_j s_{j,\rm AMPA}, \quad (3)$$

$$I_{i,\rm GABA} = (V_i - V_{\rm I}) \sum_j p_{j,\rm GABA} g_{ji,\rm GABA} s_{j,\rm GABA}, \quad (4)$$

where V_i is the membrane potential, $V_{\rm E} = 0$ mV and $V_{\rm I} = -70$ mV are reversal potentials for excitatory and inhibitory synapses, respectively. The extracellular magnesium concentration ($[{\rm Mg}^{2+}]$) is set to 1 mM.[16] g_{ji} labels the maximum synaptic conductance from neuron j to neuron i, depending on ion channels and cell pairs. s_j denotes the gating variable. p_j represents the synaptic efficacy with short-term plasticity, as will be described in Subsection 2.2.

Given a spike train $\{t_k\}$ in the presynaptic neuron j, the gating variables $s_{j,\rm AMPA}$ and $s_{j,\rm GABA}$ follow the first-order dynamics:[7]

$$\frac{{\rm d}s_{j,\rm GABA}(t)}{{\rm d}t} = -\frac{s_{j,\rm GABA}(t)}{\tau_{\rm GABA}} + \sum_k \delta(t - t_k), \quad (5)$$

with $\tau_{\rm GABA} = 10$ ms, and

$$\frac{{\rm d}s_{j,\rm AMPA}(t)}{{\rm d}t} = -\frac{s_{j,\rm AMPA}(t)}{\tau_{\rm AMPA}} + \sum_k \delta(t - t_k), \quad (6)$$

with $\tau_{\rm AMPA} = 2$ ms. $s_{j,\rm NMDA}$ obeys much slower, second-order dynamics:

$$\frac{{\rm d}s_{j,\rm NMDA}(t)}{{\rm d}t} = -\frac{s_{j,\rm NMDA}(t)}{\tau_{\rm NMDA}} + \alpha_{\rm NMDA} x_j(t)\left(1 - s_{j,\rm NMDA}(t)\right), \quad (7)$$

$$\frac{{\rm d}x_j(t)}{{\rm d}t} = -\frac{x_j(t)}{\tau_x} + \sum_k \delta(t - t_k), \quad (8)$$

with $\tau_{\rm NMDA} = 100$ ms, $\alpha_{\rm NMDA} = 0.5$ kHz, and $\tau_x = 2$ ms.

The strength of recurrent connectivity between neurons simply depends on the difference between their preferred directions: $W_{ij} = W(\theta_i - \theta_j)$; correspondingly, $g_{ij} = W_{ij} G$, with $G^{\rm E\to E} = 1.09$ nS, $G^{\rm E\to I} = 0.846$ nS, $G^{\rm I\to E} = 1.336$ nS and $G^{\rm I\to I} = 1.024$ nS. $W(\theta_i$–$\theta_j)$ is normalized, obeying

$$\frac{1}{360}\int_0^{360} W(\theta_i - \theta_j)\,{\rm d}\theta_j = 1. \quad (9)$$

Without loss of generality, we assume a uniform connectivity strength profile, except for the connections between pyramidal cells: $W^{\rm E\to I} = 1.0$, $W^{\rm I\to E} = 1.0$, $W^{\rm I\to I} = 1.0$, and

$$W_{ij}^{\rm E\to E} = J_-^{\rm E\to E} + \left(J_+^{\rm E\to E} - J_-^{\rm E\to E}\right) \times \exp\left[-(\theta_i - \theta_j)^2/(2\sigma_{\rm EE}^2)\right], \quad (10)$$

where $J_-^{\rm E\to E}$ and $J_+^{\rm E\to E}$ denote the strength of contralateral and ipsilateral connectivity, respectively, and $\sigma_{\rm EE}$ is the connectivity width. $J_+^{\rm E\to E} = 1.62$, $\sigma_{\rm E\to E} = 18°$, and $J_-^{\rm E\to E}$ is determined by Eq. (9).

The background activity is modeled as an independent Poisson spike train with a frequency of 1.8 kHz (given 1000 presynaptic neurons, then each neuron fires independently at 1.8 Hz). The corresponding synaptic conductance ($G_{\rm ext}$) is 3.1 nS and 2.38 ns for pyramidal cells and interneurons, respectively.

2.2. Short-term plasticity

The short-term plasticity is modeled based on the synaptic efficacy adaptation at pre-synapses.[12] Let u be the current release probability of neurotransmitters and v be the fraction of resources available for depletion; the instantaneous synaptic efficacy is thus depicted by $p = uv$. When a spike occurs, the release probability increases due to the flux of calcium into the axon terminal, which acts as a mechanism of short-term facilitation. Meanwhile, a portion of the remaining resources is utilized for chemical transmission, causing v to decrease and function as the short-term depression component. Between spikes, u decays over time with a timescale of $\tau_{\rm F}$, while the replenishment of neurotransmitters occurs with a time constant of $\tau_{\rm D}$. Overall, the dynamics of STP can be described as follows:

$$\begin{aligned}\frac{{\rm d}u}{{\rm d}t} &= \frac{U-u}{\tau_{\rm F}} + U(1-u)\delta\left(t-t_{\rm sp}\right),\\ \frac{{\rm d}v}{{\rm d}t} &= \frac{1-v}{\tau_{\rm D}} - uv\delta\left(t-t_{\rm sp}\right),\end{aligned} \tag{11}$$

where $t_{\rm sp}$ denotes the spike timing, and U ($0 < U \leq 1$) controls the baseline strength as well as the amplification effect caused by a spike. An STF-dominated synapse is characterized by low U and $\tau_{\rm F} \gg \tau_{\rm D}$, while an STD-dominated synapse usually suffers from depletion of neurotransmitters with $\tau_{\rm D} \gg \tau_{\rm F}$. Considering that pyramidal cells in the PFC generally exhibit STF,[8,17] we assume that STP emerges only at recurrent excitatory synapses for simplicity, i.e., $p_{j,\rm GABA} \equiv 1$ and $p_{j,\rm NMDA} \equiv u_j v_j$. All simulations were conducted under $U = 0.2$ and $\tau_{\rm F} \gg \tau_{\rm D}$.

2.3. Population firing profile

The population firing profile (PFP) during the delay period is often used to characterize the overall state of the network, involving the firing rates of all pyramidal cells over each bin of 10 ms.[18] Worthy of attention are its height $H_{\rm PFP}$ and sharpness $S_{\rm PFP}$. $H_{\rm PFP}$ labels the difference in firing rate between the neurons whose preferred directions are around the cue direction and those whose directions are opposite the cue direction, i.e.,

$$H_{\rm PFP} = f_{\rm cue} - f_{\rm opp}. \tag{12}$$

$S_{\rm PFP}$ resembles the kurtosis describing probability density functions and is defined as

$$S_{\rm PFP} = \frac{\left(\sum_{i=1}^{N_{\rm E}} f_i \cdot (\theta_i - \theta_{\rm c})^4\right) \Big/ \left(\sum_{i=1}^{N_{\rm E}} f_i\right)}{\left[\left(\sum_{i=1}^{N_{\rm E}} f_i \cdot (\theta_i - \theta_{\rm c})^2\right) \Big/ \left(\sum_{i=1}^{N_{\rm E}} f_i\right)\right]^2}, \tag{13}$$

where f_i and θ_i are the firing rate and preferred direction of cell i, and $\theta_{\rm c}$ is the cue direction. $S_{\rm PFP}$ is equal to 1.8 for the plateau-like profile and 3.0 for the standard Gaussian curve.

To track the memory state in the network, a population activity vector $\boldsymbol{P}$ is used to infer the peak location of the bump attractor during a given time interval,

$$\boldsymbol{P}(t) = \sum_{i=1}^{N_{\rm E}} \boldsymbol{F}_i(t), \tag{14}$$

where $\boldsymbol{F}_i$ is a vector, with direction θ_i and amplitude representing the average firing rate of neuron i during the 500 ms bin centered on time t. The angle of $\boldsymbol{P}$, $\theta_{\rm P}$, represents the remembered cue direction, subject to drifts caused by the randomness of background inputs. The length of $\boldsymbol{P}$, $L_{\rm P}$, somewhat reflects the strength of memory storage.

3. Results

3.1. Short-term plasticity at single synapses

To clarify the impact of STP on WM, we first investigated the synaptic plasticity at single synapses. For fixed U ($= 0.2$), the synaptic plasticity is modulated by $\tau_{\rm F}$, $\tau_{\rm D}$ and the firing rate f of the presynaptic neuron. Given that the synaptic efficacy $p = uv$ is equal to U at the resting state, the synapse exhibits facilitation for $p > U$ and otherwise depression. When the neuron periodically discharges at 3 Hz, u and v undergo a series of pulses; with each spike, u increases instantly and then declines gradually, while v displays the opposite pattern [Fig. 2(a)].

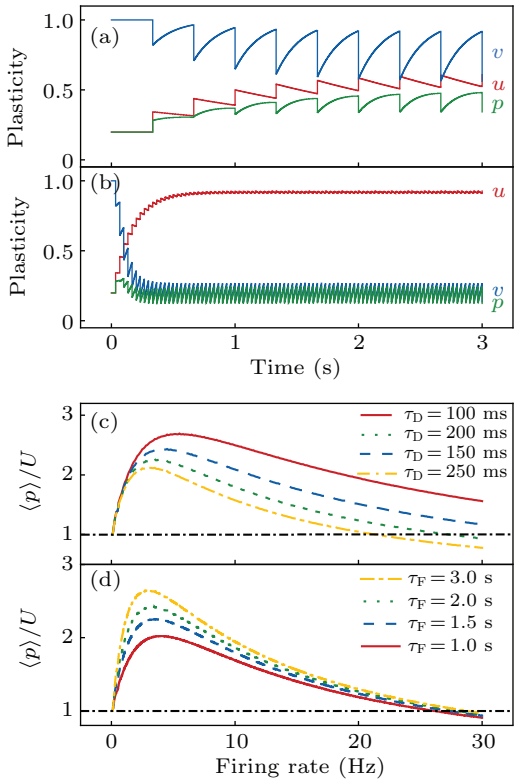


Fig. 2. Strength of synaptic plasticity under various conditions. (a) and (b) Time courses of u (pink), v (blue) and p (green) with $\tau_{\rm D} = 200$ ms, $\tau_{\rm F} = 1.5$ s and the firing rate of 3 Hz (a) or 30 Hz (b). (c) Time-averaged p/U as a function of firing rate for different $\tau_{\rm D}$ values, with $\tau_{\rm F}$ fixed at 1.5 s. The synapse shows facilitation if the ratio is greater than one. (d) Time-averaged p/U as a function of firing rate for various $\tau_{\rm F}$ values with $\tau_{\rm D} = 200$ ms.

After seven spikes, u and v vary periodically, and thus p oscillates between 0.34 and 0.49. Overall, this represents synaptic facilitation. However, when the firing rate reaches 30 Hz, u and v change periodically after only eight spikes (much earlier in time), and p fluctuates between 0.12 and 0.24 [Fig. 2(b)]; in this case, the synapse demonstrates overall depression.

To further reveal the dependence of synaptic efficacy on f, τ_F and τ_D, we calculated the average of p over one full period, $\langle p \rangle$. It first increases and then decreases with increasing f at fixed τ_F and τ_D; the peak shifts rightwards and its height elevates with decreasing τ_D [Fig. 2(c)]. In contrast, the peak shifts leftwards and becomes higher with increasing τ_F [Fig. 2(d)]. Note that $\langle p \rangle > U$ occurs over a relatively wide range of f, which is more prominent at larger τ_F and smaller τ_D. Together, given $\tau_F \gg \tau_D$, synaptic facilitation can be achieved when the firing rate is not high; increasing τ_F or decreasing τ_D always enhances the synaptic facilitation.

3.2. Maintenance of working memory with STP

The results above indicate that τ_F and τ_D exert opposing controls over STP. In the following, τ_D is typically set at 200 ms unless otherwise specified in Subsection 3.4, while τ_F is varied to explore the impact of synaptic plasticity on the maintenance of visuospatial working memory. Before cue presentation, the network exhibits homogenous sparse firing at a few Hz [Fig. 3(a)]. Given the cue located at $\theta_c = 180°$, the neurons with preferred directions around θ_c are activated to persistently discharge during the delay period, while others with preferred directions far away from θ_c are greatly suppressed. Thus, a bump attractor is maintained to encode the cue location, which is attributed to the slow recurrent excitation driven by NADARs and strong global inhibition mediated by GABARs.[7]

We calculated the mean firing rate of each pyramidal cell over the whole delay period and obtained the population firing profile, which is bell shaped with the maximum around θ_c and varies remarkably with τ_F [Fig. 3(b)]. The peak height elevates and the peak width enlarges with increasing τ_F due to enhanced synaptic transmission. Quantitatively, the PFP can be characterized by its height H_{PFP} and sharpness S_{PFP}; with increasing τ_F, H_{PFP} increases towards saturation, while S_{PFP} first increases and then decreases [Fig. 3(c)].

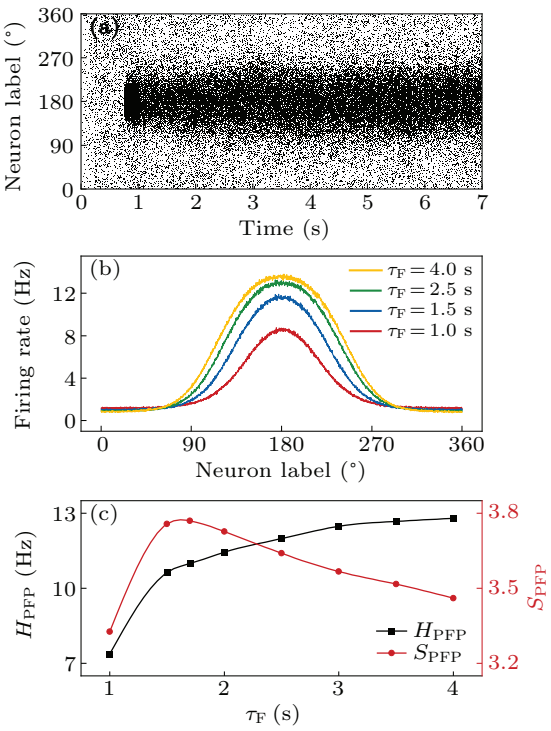


Fig. 3. Spatiotemporal firing patterns of pyramidal cells with $\tau_D = 200$ ms. (a) Raster plot for principal cells with $\tau_F = 1.5$ s when a cue is presented at 180° from 750 ms to 1.0 s. There are 2048 pyramidal cells labeled by their preferred directions and arranged along the y-axis in order. Dots on each row mark spikes of that neuron. (b) Population firing profiles for different τ_F values. The firing rate of each pyramidal cell is an average over the whole delay period and over 100 trials. (c) Height (square) and sharpness (circle) of the population firing profile versus τ_F.

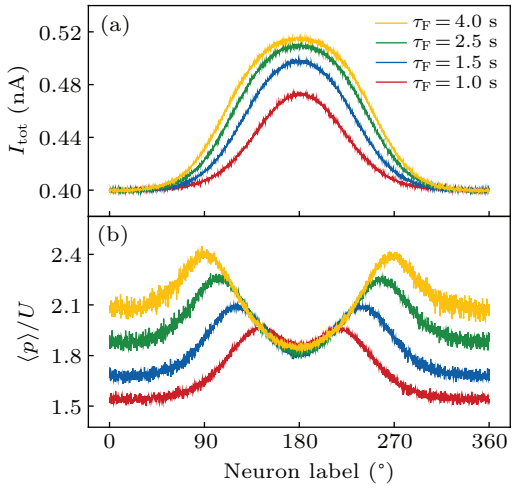


Fig. 4. Synaptic mechanism for persistent activity during the delay period. (a) Total current and (b) synaptic plasticity (averaged over the delay period) for each pyramidal cell for different τ_F values with $\tau_D = 200$ ms.

The changing trend described above can be understood as follows. The short-term plasticity modulates the balance between excitation and inhibition in the network. As can be seen in Fig. 4(a), the total current (I_{tot}) for each neuron within the bump attractor increases with greater τ_F. At $\tau_F = 500$ ms, I_{tot} is relatively uniform across the pyramidal cells (data not shown), and no bump attractor emerges. For $\tau_F \geq 1.0$ s, stronger short-term facilitation leads to the activation of more neurons firing at higher rates. This enhanced local excitation activates more neurons near the edges of the attractor. Since synaptic facilitation becomes limited at high firing rates (Fig. 2), the highest synaptic efficacy does not appear around θ_c but rather on either side of θ_c, especially at larger τ_F values [Fig. 4(b)]. Thus, the curve of I_{tot} versus neuron index becomes wider and flatter around θ_c as τ_F increases. This leads to a decrease in S_{PFP} at large τ_F. Overall, larger τ_F values give rise to stronger synaptic

efficacy, resulting in higher H_{PFP}, but cause the current profile to broaden, thereby constraining S_{PFP}.

3.3. Robust memory storage and sensitivity to cue presentation

The robustness of bump attractor dynamics is crucial for working memory, making it necessary to investigate its stability over time, specifically its resistance to random drifts and distractions. Due to the circular symmetry in synaptic connectivity strength and randomness of background inputs, the peak location of the bump attractor (θ_{P}) shifts randomly over time, resembling a diffusion process [Fig. 5(a)]. We conducted 100 simulations of the same mnemonic task and calculated the standard deviation of θ_{P}, σ_{P}. Although σ_{P} tends to increase across the delay period, its magnitude is sufficiently small (around 9° at 6 s) [Fig. 5(b)], which is attributed to STF. Indeed, σ_{P} at 6 s decreases with increasing τ_{F} [Fig. 5(c)]. Nevertheless, the decline becomes less pronounced for $\tau_{\mathrm{F}} > 2.5$ s, suggesting a limited role for simply enhancing STF. Overall, STF plays a beneficial role in mitigating the random drift of the bump attractor.

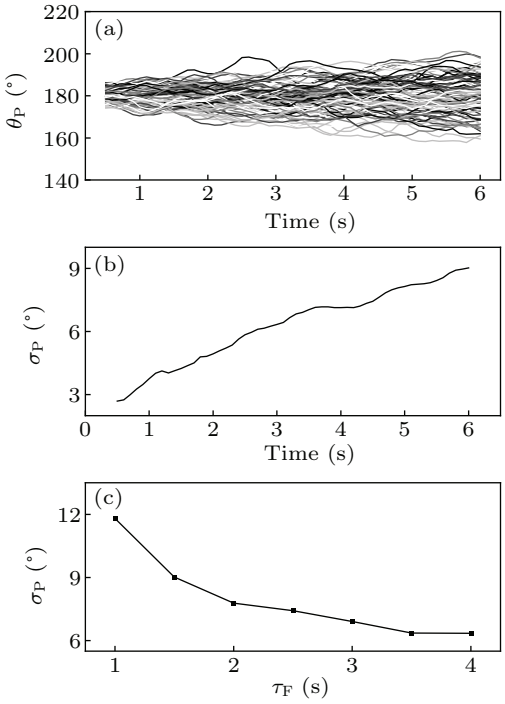


Fig. 5. Random drifts of the bump attractor during the delay period with $\tau_{\mathrm{D}} = 200$ ms. (a) Time courses of the angle of the population activity vector on 100 simulations for $\tau_{\mathrm{F}} = 1.5$ s. (b) Temporal evolution of the standard deviation of θ_{P}, σ_{P}. The data are from the same simulations as in (a). (c) σ_{P} at 6 s versus τ_{F}.

The resistance of the bump attractor against a distractor also reflects its dynamic stability. The distractor-related input has the same strength and duration as the cue-related input. Specifically, the cue is presented at $\theta_{\mathrm{c}} = 90°$, while the distractor is presented at θ_{d} (somewhere between 90° and 270°) from 3.75 s to 4 s. After the removal of the distractor, three scenarios may emerge: 1) the bump attractor centers around θ_{d}, leading to memory loss [Fig. 6(a)]; 2) the bump attractor remains centered around θ_{c}, preserving the memory of the cue [Fig. 6(b)]; 3) the center of the bump attractor lies between θ_{d} and θ_{c}, resulting in a bias in cue memory [Fig. 6(c)]. The occurrence of each scenario depends on various factors, such as background inputs, the angular difference between the cue and distractor ($\theta_{\mathrm{cd}} = |\theta_{\mathrm{d}} - \theta_{\mathrm{c}}|$), τ_{F} and τ_{D}. To quantify the deviation of memory storage, we calculated the difference in θ_{P} before and after the distractor presentation, denoted as $\Delta\theta = |\theta_1 - \theta_2|$. Considering the slow process of synaptic plasticity, θ_1 represents the peak location of the bump attractor right before the distractor onset, while θ_2 is that at 3 s after the distractor offset. An average of $\Delta\theta$ over 100 trials is also taken and denoted as $\overline{\Delta\theta}$.

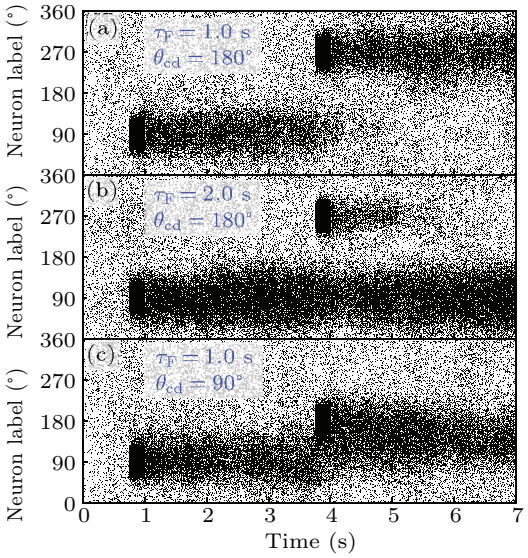


Fig. 6. Spatiotemporal firing patterns of cells in the presence of a distractor with $\tau_{\mathrm{D}} = 200$ ms. Examples of memory loss for $\tau_{\mathrm{F}} = 1.0$ s and $\theta_{\mathrm{cd}} = 180°$ (a), perfect memory maintenance for $\tau_{\mathrm{F}} = 2.0$ s and $\theta_{\mathrm{cd}} = 180°$ (b), and partial distraction for $\tau_{\mathrm{F}} = 1.0$ s and $\theta_{\mathrm{cd}} = 90°$ (c).

For $\theta_{\mathrm{cd}} = 45°$ or 90°, although the cue- and distractor-related inputs share the same strength and duration, it is generally more difficult to evoke and maintain a new bump attractor around θ_{d}, especially at large τ_{F} values, due to the enhanced local excitation around the existing bump attractor and the dominance of global inhibition [Fig. 7(a)]. Indeed, only scenarios 2 and 3 appear for $\tau_{\mathrm{F}} > 1.0$ s, and the likelihood of scenario 2 improves with increasing τ_{F} [Fig. 7(c)]. For $\theta_{\mathrm{cd}} = 135°$ or 180°, the pyramidal cells around θ_{d} may be easily activated to win the competition with the prior bump attractor at $\tau_{\mathrm{F}} = 1.0$ s [Fig. 7(b)]. However, at $\tau_{\mathrm{F}} = 2.0$ s, only scenarios 3 and 2 emerge for $\theta_{\mathrm{cd}} = 135°$ and 180°, respectively [Fig. 7(c)].

Figure 7(d) shows the dependence of $\overline{\Delta\theta}$ on θ_{cd} and τ_{F}. At $\theta_{\mathrm{cd}} = 90°$, $\overline{\Delta\theta}$ first declines markedly and then gradually tends towards saturation with increasing τ_{F} (see the inset). The saturation occurs because the release probability u cannot increase beyond 1, limiting the extent of STF. For fixed τ_{F},

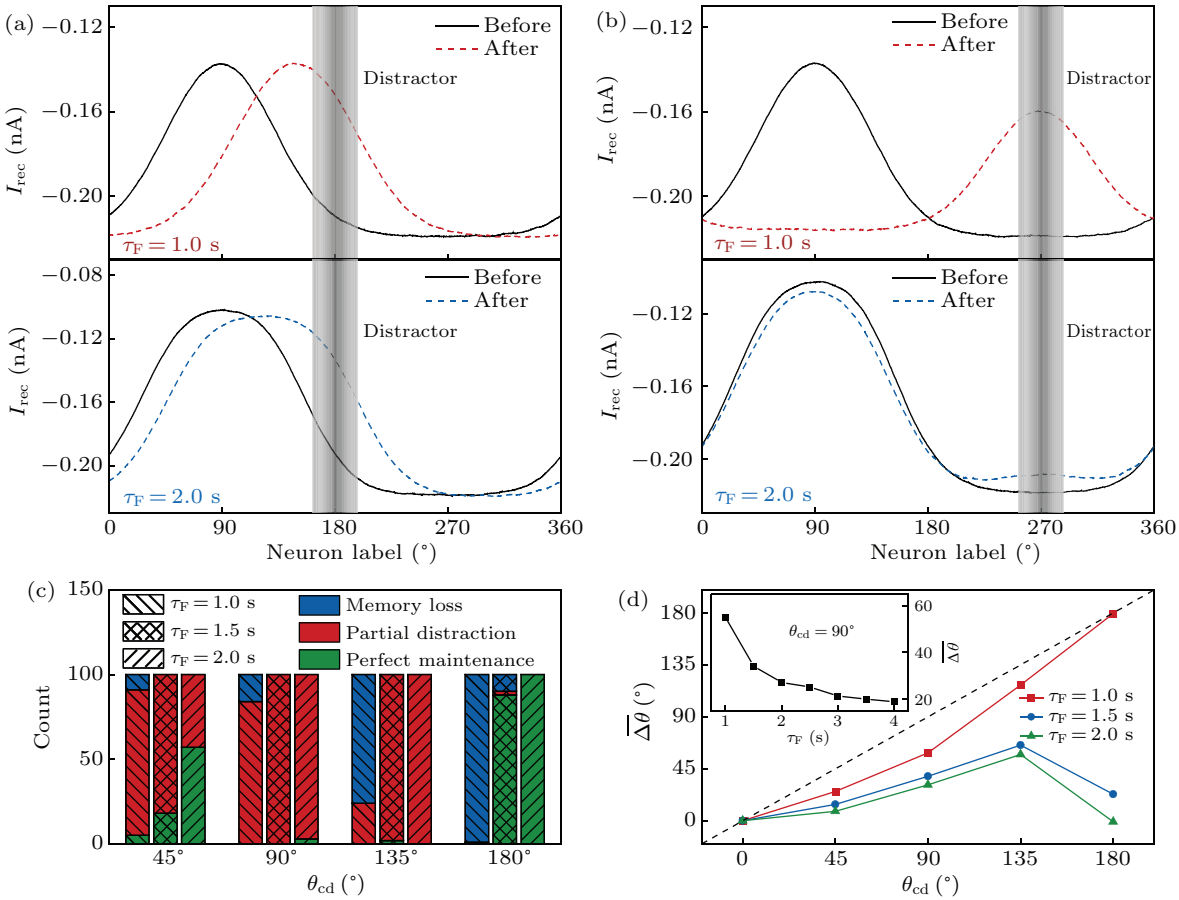


Fig. 7. Resistance of memory storage against distraction with STF. (a) and (b) The average of recurrent currents over 100 trials for each pyramidal cell before (solid line) and after (dashed line) distraction for $\tau_F = 1.0$ s (upper) or 2.0 s (lower) and $\theta_{cd} = 90°$ (a) or 180° (b). The gray rectangle marks the distractor position. (c) Distribution of three scenarios for different θ_{cd} and τ_F values. Here, memory loss and perfect maintenance separately correspond to $\Delta\theta/\theta_{cd} \geq 0.8$ and $\Delta\theta/\theta_{cd} \leq 0.2$. (d) $\overline{\Delta\theta}$ versus θ_{cd} for different τ_F values. The inset shows $\overline{\Delta\theta}$ versus τ_F with $\theta_{cd} = 90°$.

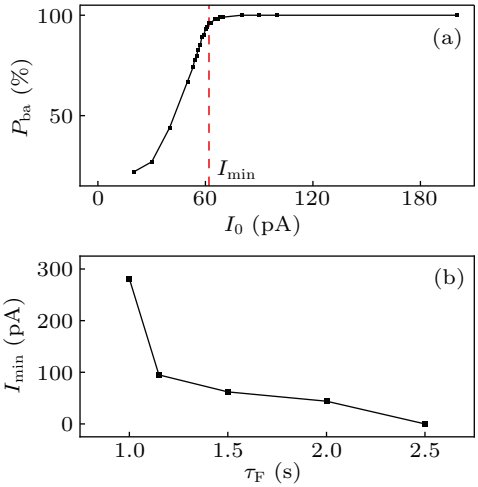


Fig. 8. Short-term facilitation sensitizes the cue detection with $\tau_D = 200$ ms. (a) Occurrence probability of the memory state as a function of I_0 for $\tau_F = 1.5$ s. I_{min} refers to the minimal strength that satisfies $P_{bump} \geq 0.95$. (b) I_{min} versus τ_F.

$\overline{\Delta\theta}$ increases with increasing θ_{cd} up to 135°; at $\theta_{cd} = 180°$, $\overline{\Delta\theta}$ depends remarkably on τ_F. Increasing τ_F facilitates reducing the deviation, especially at $\theta_{cd} = 180°$. Altogether, the network's robustness against drift and distraction is enhanced with larger τ_F.

In addition to the attractor stability, the network's sensitivity to cue presence is also worth probing. As mentioned earlier, $I_0 = 500$ pA is sufficient for a cue to evoke a bump attractor, where the mean and variance of L_P are denoted as $m_{L,500}$ and $\sigma_{L,500}$, respectively. Regardless of the cue intensity, only states with $L_P > L_{th}$ $(= m_{L,500} - 3\sigma_{L,500})$ are regarded as memory states.[18] The occurrence probability of the memory state quickly increases towards saturation with increasing I_0 [Fig. 8(a)], and the minimum strength required for 95% occurrence is labeled as I_{min}. At $\tau_D = 200$ ms, I_{min} decreases with increasing τ_F [Fig. 8(b)]. This heightened sensitivity to cues still stems from the enhancement of synaptic efficacy. Note that I_{min} approaches zero at $\tau_F = 2.5$ s, indicating that the network is hypersensitive. Without cue inputs, the STF is sufficiently strong with high τ_F, allowing certain pyramidal cells to predominate over others when activated by random background inputs. This, along with strong recurrent excitation and global inhibition from interneurons, can lead these cells to discharge persistently. In this case, the attractor center becomes entirely random. This result suggests a potential side effect of excessive STF.

3.4. Enhancing STD deteriorates the WM performance

We have probed the network behavior by varying τ_F while keeping τ_D fixed at 200 ms. Here, we further examined how working memory is affected by varying the time constant of short-term depression. As τ_D increases, the profile of the bump attractor becomes lower, while suppressed pyramidal cells beyond the attractor instead elevate their firing activity [Fig. 9(a)]. Accordingly, H_{PFP} decreases with increasing τ_D, while S_{PFP} first increases and then decreases [Fig. 9(b)]. The minimal cue strength required for the memory state also increases with increasing τ_D [Fig. 9(c)], indicating a reduced sensitivity to cue detection. The random drifts of the bump attractor become more prominent with increasing τ_D [Fig. 9(d)]. When the angular difference between the cue and distractor is 90°, $\overline{\Delta\theta}$ also increases with increasing τ_D [Fig. 9(d)]. In contrast to τ_F, increasing τ_D weakens the robustness of working memory and the network's sensitivity to cue presentation.

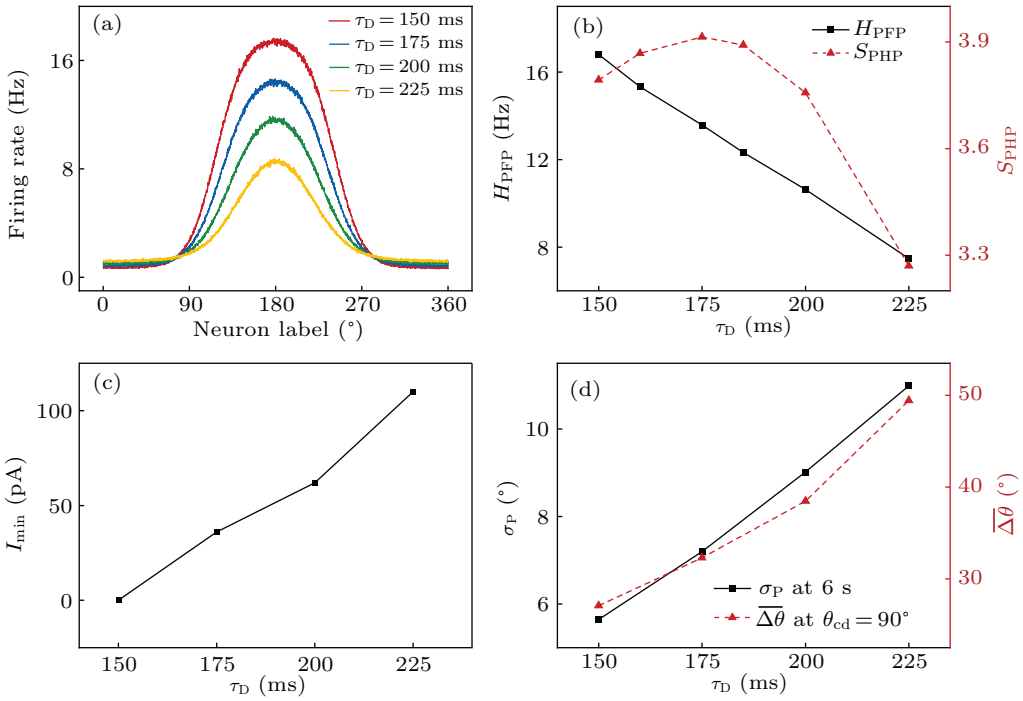


Fig. 9. Network behavior with $\tau_F = 1.5$ s. (a) Population firing profile for different τ_D values and (b) the corresponding H_{PFP} and S_{PFP} versus τ_D. The firing rate is averaged over the whole delay period and over 100 simulations. (c) I_{min} versus τ_D. (d) σ_P at 6 s (diamond) and $\Delta\theta$ with $\theta_{cd} = 90°$ (triangle) versus τ_D.

Indeed, τ_D and τ_F exert opposing controls over transmission efficacy and ultimately on working memory performance. Lower τ_D ensures a continuous supply of neurotransmitters over time, enhancing the synaptic efficacy, whereas higher τ_D results in a neurotransmitter shortage, reducing the efficacy; higher τ_D has a similar effect to lower τ_F in terms of limiting the efficacy. Consequently, τ_D and τ_F have opposite influences on the short-term plasticity. As a result, lower τ_D strengthens the robustness of working memory, similar to higher τ_F.

4. Discussion

In this study, we systematically examined the impact of short-term plasticity on working memory in the oculomotor delayed response task. Short-term plasticity comprises two components: short-term facilitation, which enhances the neurotransmitter release probability, and short-term depression, which restricts the depletion of neurotransmitters from recovery. These two components act in opposition at the single synapse level. Consistently, increasing τ_F or decreasing τ_D enhances the memory maintenance and sensitivity to cue detection. Compared to STD, excessively strong STF can render the network hypersensitive, while inadequate STF can result in the loss of the mnemonic state during the delay period. Suitable levels of STP are crucial for the network's performance.

Numerous studies have demonstrated the role of STF in enhancing the stability of WM. For instance, STF markedly reduces the drifts caused by connectivity heterogeneity in a WM network.[19] STP improves network stability when the network suffers from synaptic connectivity defects.[20] Noise resistance can be improved when decoding a continuous attractor neural network with STF.[21] Differently, the current study offered a detailed analysis of network behavior over a wide range of STF levels and provides novel insight into the network's stability against drifts and distractions and sensitivity to cue detection.

In a firing rate-based network model, STF and STD exert opposing effects on drifts caused by random firing or connectivity heterogeneity.[13] The current study confirms the contrasting functions of STF and STD and further investigated

the network's response to distractors and its sensitivity to cue presentation. Note that stronger STF alone leads to increased drifts when the effects of τ_D-controlled STD are neglected.[9] Without STD, the synaptic efficacy improves monotonically towards saturation at individual synapses with increasing τ_F, and the profile of synaptic efficacy around the cue position is a plateau at higher τ_F, which amplifies local excitation and drives more neurons to fire at higher rates. Thus, the attractor is more prone to shift due to random background inputs. With both STF and STD in our study, however, the synaptic efficacy profile exhibits two peaks on either side of the cue direction, counteracting each other; this aids in preventing the attractor from drifting.

The sensitivity to cue presentation has a crucial role in WM. Mejias *et al.*[22] reported that STF improves information retrieval in noisy neural networks. Consistent with theirs, our simulations showed a decrease in the minimal cue strength required for the memory state with increasing τ_F. However, at extremely high τ_F, the WM network still exhibits a mnemonic state even without a cue, resulting in a loss of cue detection. Therefore, achieving optimal WM performance necessitates a moderate level of STF, which enhances weak signal detection while preserving the ability to discriminate between cues and noise.

While the short-term facilitation mechanism in neural networks may share similarities with the excitation mediated by NMDA receptors, there are three key differences to highlight. First, the time scale of NMDARs ranges from tens to hundreds of milliseconds,[23] whereas STF can persist for minutes.[24] Second, NMDAR-mediated postsynaptic currents are voltage dependent and follow a second-order gating process, ultimately decaying to zero.[7] In contrast, STF involves the release of neurotransmitters from presynaptic vesicles, which is influenced by the release probability and available resources. The baseline release probability in the absence of presynaptic firing is U (nonzero). Third, NMDARs play an indispensable role in working memory, and impairments in NMDA function directly affect WM performance.[25] In contrast, while STF is known to reduce random drifts,[19] enrich neural firing patterns[26] and introduce interference from preceding trials,[10] it is not essential for the formation of attractors in WM networks. Instead, STF modulates WM by influencing its dynamics and performance.

The influence of short-term plasticity on working memory extends beyond its known complexity and functionality. Only the STP of NMDAR-driven currents is considered in our simulations, and the modulation of working memory could be further enriched by considering the STP of AMPAR- and GABAR-mediated currents. In addition, exploring other forms of STP holds promise for further insight. Developing a more comprehensive model would enable a deeper understanding and interpretation of complex cognitive tasks.

Acknowledgement

This study was supported by STI 2030-Major Projects 2021ZD0201300.

References

[1] Baddeley A 1992 *Science* **255** 556
[2] Miller E K 2000 *Nat. Rev. Neurosci.* **1** 59
[3] Miller E K and Cohen J D 2001 *Annu. Rev. Neurosci.* **24** 167
[4] Cowan N 2014 *Educ. Psychol. Rev.* **26** 197
[5] Funahashi S, Bruce C J and Goldman-Rakic P S 1989 *J. Neurophysiol.* **61** 331
[6] Takeda K and Funahashi S 2002 *J. Neurophysiol.* **87** 567
[7] Compte A, Brunel N, Goldman-Rakic P S and Wang X J 2000 *Cereb. Cortex* **10** 910
[8] Hempel C M, Hartman K H, Wang X J, Turrigiano G G and Nelson S B 2000 *J. Neurophysiol.* **83** 3031
[9] Pereira J and Wang X J 2015 *Cereb. Cortex* **25** 3586
[10] Kilpatrick Z P 2018 *Sci. Rep.* **8** 7879
[11] Barbosa J, Stein H, Martinez R L, Galan-Gadea A, Li S, Dalmau J, Adam K C S, Valls-Solé J, Constantinidis C and Compte A 2020 *Nat. Neurosci.* **23** 1016
[12] Mongillo G, Barak O and Tsodyks M 2008 *Science* **319** 1543
[13] Seeholzer A, Deger M and Gerstner W 2019 *PLoS Comput. Biol.* **15** e1006928
[14] Lisman J E, Fellous J M and Wang X J 1998 *Nat. Neurosci.* **1** 273
[15] Wang X J 1999 *J. Neurosci.* **19** 9587
[16] Jahr C E and Stevens C F 1990 *J. Neurosci.* **10** 3178
[17] Wang Y, Markram H, Goodman P H, Berger T K, Ma J and Goldman-Rakic P S 2006 *Nat. Neurosci.* **9** 534
[18] Wang T, Sun J, Yang F, Li J, Wang W and Liu F 2021 *Phys. Rev. E* **104** 024416
[19] Itskov V, Hansel D and Tsodyks M 2011 *Front. Comput. Neurosci.* **5** 40
[20] Kozachkov L, Tauber J, Lundqvist M, Brincat S L, Slotine J J and Miller E K 2022 *PLoS Comput. Biol.* **18** e1010776
[21] Fung C C A, Wong K Y M, Wang H and Wu S 2012 *Neural Comput.* **24** 1147
[22] Mejias J, Hernandez-Gomez B and Torres J J 2012 *Europhys. Lett.* **97** 48008
[23] Hestrin S, Nicoll R A, Perkel D J and Sah P 1990 *J. Physiol.* **422** 203
[24] Zucker R S and Regehr W G 2002 *Annu. Rev. Physiol.* **64** 355
[25] Tsukada H, Nishiyama S, Fukumoto D, Sato K, Kakiuchi T and Domino E F 2005 *Neuropsychopharmacology* **30** 1861
[26] Hansel D and Mato G 2013 *J. Neurosci.* **33** 133